

Development of a Straightness Monitor Using Laser Interferometry

Matthew Lucia

2008 NSF/REU Program
Physics Department, University of Notre Dame

In Collaboration With:
Zachary Liptak
AJ McGauley
Thomas Rehagen

Advisor:
Dr. Michael Hildreth

1 Abstract

The international linear collider (ILC) is a proposed particle accelerator designed to further physicists' understanding of particle physics on the TeV energy scale. In the ILC, particle beam energy will be determined by measuring the beam deflection through a chicane of magnets and a series of beam position monitors (BPMs). The main focus of this work was the development of a prototype laser interferometry system to measure the stability of the entire system. With the use of a heterodyne laser, position of the BPMs—with respect to the particle beam—can be established on the order of $50nm$, enough precision for reliable energy measurements. A computer simulation was designed and tested to help with the development of the system. Work progressed on both a transverse beamline motion monitor and a transverse laser motion monitor. At the time of this writing, a working upgraded model of the former monitor has been completed, but the technique used for the latter monitor was proved flawed.

2 Underlying Physics

2.1 Standard Model and Beyond

The Standard Model has been one of the great successes of particle physics over the past half-century. However, despite numerous experimental verifications of its various predictions, many physicists believe that the Standard Model is incomplete. In particular, mysteries concerning electroweak symmetry breaking and the origin of mass have led to the conjecture of one final particle in the Standard Model, the so-called Higgs boson. Other puzzles, such as the oscillation of neutrino flavors and the hypothesized existence of dark matter, even seem to call for physical theories beyond those provided by the Standard Model. These mysteries of particle physics can only be probed with incredibly high energies, requiring the construction of increasingly powerful particle accelerators. The most powerful accelerator at the time of this writing is the Tevatron, a proton-antiproton collider located at Fermi National Laboratory, outside of Chicago. At full power, it falls just shy of the theoretical lower bound on the Higgs boson energy.

2.2 Large Hadron Collider

The Large Hadron Collider (LHC) is a proton-proton collider under the final stages of completion near Geneva on the Swiss-French border. Once running, the 27-kilometer circular accelerator will be capable of producing collisions with energies seven times higher than those in the Tevatron. At these energies, the LHC should be able to cover the entire theoretical range for mass of the Higgs boson, making its detection highly probable. With such an energy upgrade, experimental evidence for such theories as supersymmetry and string theory may also surface. Circular particle accelerators like the LHC are so-designed for one important reason: Charged particles bend in circular orbits in the presence of a uniform magnetic field. Large

superconducting magnets can therefore be used to bend the protons in circular paths while kinetic energy is added via an electric potential.

Infinite increase of energy by this method is prohibited by synchrotron radiation, electromagnetic radiation produced by accelerating charged particles. Using the Larmor formula (Eq. 1) with the relativistic centripetal acceleration (Eq. 2) in particle accelerators, one finds that the rate of energy loss is inversely proportional to r^2 , the square of the accelerator ring's radius, and directly proportional to γ^4 , the fourth power of the particle's Lorentz factor (Eq. 3):

$$P_{Larmor} = \frac{e^2}{6\pi\epsilon_0 c^3} a^2 \quad (1)$$

$$a_c = \frac{\gamma^2 v^2}{r} \approx \frac{\gamma^2 c^2}{r} \quad (v \approx c) \quad (2)$$

$$P_{synch} = \frac{e^2 c}{6\pi\epsilon_0} \frac{\gamma^4}{r^2} \quad (3)$$

Thus, an upper bound of energy exists where the energy added by the accelerator is exactly in equilibrium with the energy lost to synchrotron radiation. Synchrotron radiation is minimized by building accelerator rings with larger radii, the key reason why—everything else equal—the larger proton-proton LHC can reach higher energies than can the smaller proton-antiproton Tevatron.

2.3 International Linear Collider

2.3.1 Need for a Linear Collider

Both the Tevatron and the LHC use protons or antiprotons, but these are baryons, composite particles composed of several fundamental particles. When they collide in an accelerator, the actual interaction is between two individual quarks or gluons. The remaining constituent particles of the baryons do not directly participate in the collision, but they serve to

make the data readout extremely messy. The ideal solution would be collisions between fundamental particles, which would yield much cleaner and more understandable results. However, free quarks have never been observed, and muons decay too quickly, and neutrinos interact too weakly, so electrons and positrons are the only remaining option.

Returning to the formula for synchrotron radiation, we see that the factor of γ^4 is extremely important when comparing protons and electrons. Since a proton is about 1836 times more massive than an electron, an electron will radiate with $(1836)^4 = 1.136 \times 10^{13}$ times the power of a proton with the same kinetic energy and radius of curvature. Consequently, circular particle accelerators cannot electrons beyond energies much higher than 100GeV, the energy of the former Large Electron Positron collider at CERN. The solution is a linear particle accelerator, in which charged particles do not undergo centripetal acceleration and thus do not radiate. However, a linear accelerator poses different challenges. The beam of electrons must be accelerated in one pass, rather than gradually with each circuit, so the accelerator must be long and powerful. Indeed, the plans for the ILC call for a $40km$ beamline with an electric potential of $30 \frac{MV}{m}$ along it.

2.3.2 Beam Energy Measurement at ILC

Measurement of beam energy is another challenge in a linear particle accelerator. In a circular accelerator, the beam energy can be determined by the required magnetic field strength; moreover, measurements can be taken with each circuit, and averaging will give a very accurate value. For a linear accelerator, there are neither magnetic fields nor multiple chances to take measurements, so a different method is required. A group of scientists at University College London are currently working on a design for a chicane of four bending magnets. The magnets will be inserted into the beamline and will bend the beam out and back from its neutral position.

By measuring the transverse beam deflection and the magnetic field strength, the kinetic energy of the beam can be calculated. The position of the electron beam in the beamline is actually measured using microwave cavities called beam position monitors (BPMs). The position can be determined to within $20nm$ by analyzing the distribution of eigenmodes established within the cavity.

2.3.3 Interferometry as a Straightness Monitor

The chicane of magnets deflects the beam, but with such high beam energies, the deflection is very small, on the order of only $5mm$. Moreover, for accurate data analysis, the error on the energy can only be one part in ten thousand, so position must be measured on the order of $100nm$. The BPMs allow for measurement of the beam with respect to the beamline with this precision, but the beamline itself can vibrate by several microns during normal operation. A system for measuring the beamline's position with respect to a stationary reference point is thus required, and Dr. Michael Hildreth of the University of Notre Dame is designing such a system using laser interferometry.

3 Interferometry Optical Simulation

One project this summer was the creation of a simulation for the laser beam in the interferometer. The final laser interferometry setup will monitor each BPM on the beamline, so the laser will follow a fairly complex path. We wanted the ability to model how the laser would propagate through the various optical components. In particular, we hoped to simulate the effect of repositioning these components without having to go through the time-consuming physical realignment process. The model was designed to preemptively find and correct design flaws.

3.1 Simulation Design

For our purposes, a complicated three-dimensional system was not necessary. Taking into account the planar symmetry of the optical table, it was possible to remove the vertical axis and consider the optical pathlength on a two-dimensional xy-plane. Although some setups did involve a vertical shift, it was always a perfectly vertical translation of both interferometer arms, so it could be neglected. We also took advantage of our knowledge of the laser path to further simplify the simulation's design; specifically, since we knew the order in which the optical components would be encountered, we could leave the reflecting and refracting surfaces as infinite planes to be encountered individually. Without this simplification, much more complicated algorithms would have been necessary to determine the laser beam's path through the various optical components.

Written in C++, the simulation program kept track of the current location (as an xy-coordinate) and direction (as a polar angle) of the laser beam, as well as the current propagated pathlength. The program received an input file containing initial conditions for the beam and an ordered list of reflective and refractive surfaces. This list gave the location of the infinite planes and the change in index of refraction across the interface, the latter of which applied non-trivially only to the case of refraction. Iterating one-by-one through the optical components, the simulation first determines the location where the beam will hit the next component. It then uses either a reflection or refraction sub-function to determine the outbound angle of propagation. The simulation also tallies the total propagation pathlength from one component to the next. Once it reaches the end of the input optical components, the simulation outputs a final beam position and direction, as well as the total beam propagation pathlength.

3.2 Simulation Components

3.2.1 Reflective Surfaces

When a beam is incident on a reflective surface, it changes angle based on the Law of Reflection (Eq. 4). This is the simpler of the two types of surfaces, since the incident angle from the normal is always identical to the reflected angle from the normal. In a polar coordinate system, the reflected angle can be calculated up to a multiple of 2π as:

$$\phi_r = 2\phi_s - \phi_i \quad (4)$$

where ϕ_i is the incident angle, ϕ_r is the reflected angle, and ϕ_s is the angle of the reflective surface. Note that the simulation dealt with only planar reflecting surfaces, such as plane mirrors. Surfaces such as convex and concave mirrors were not included because they do not keep the beam collimated.

3.2.2 Refractive Surfaces

When a beam is incident on a refractive surface, it changes angle based on the Law of Refraction, Snell's Law (Eq. 5). This is the more complex of the two types of surfaces, since the change in angle depends largely on the indices of refraction of the two materials. In a polar coordinate system, the refracted angle can be calculated up to a multiple of 2π as:

$$\phi_r = \phi_s \pm \cos^{-1} \left[\frac{n_i}{n_r} \cos(\phi_i - \phi_s) \right] \quad (5)$$

where ϕ_i is the incident angle, ϕ_r is the refracted angle, ϕ_s is the angle of the refractive surface, n_i is the initial index of refraction, and n_r is the final index of refraction. Note that two answers are given by this formula, where sometimes addition and sometimes subtraction must be used. The correct angle was the angle closest to the original, since refraction never changes angle by more than ninety degrees. Also note that this simulation was designed for only flat refractive

surfaces, such as prisms. Lenses were not included because they do not keep the beam collimated. Additionally, the complicating case of total internal reflection was ignored because we intentionally avoided it in our setup.

3.2.3 Free Propagation

Propagation of the beam between surfaces was carried out using a parametric representation (Eqs. 6-8) of the intersection of two lines:

$$t_i = \frac{\sin \phi_2 (x_1 - x_2) - \cos \phi_2 (y_1 - y_2)}{\sin(\phi_1 - \phi_2)} \quad (6)$$

$$x_i = x_1 + t_i \cos \phi_1 \quad (7)$$

$$y_i = y_1 + t_i \sin \phi_1 \quad (8)$$

Where (x_1, y_1, ϕ_1) were the parameters of the beam, (x_2, y_2, ϕ_2) were the parameters of the next optical component, and (x_i, y_i, t_i) were the parameters of the intersection. Finally, the pathlength of each stage was calculated (Eq. 9) using the typical Cartesian distance formula:

$$n_1 \sqrt{(x_i - x_1)^2 + (y_i - y_1)^2} \quad (9)$$

Note that this is the optical pathlength, as the distance is weighted by the index of refraction through which the beam travels. Optical pathlength is a measure of the number of wavelengths of the light, rather than just of distance traveled.

3.3 Successes and Failures

As of this writing, the simulation program has been successfully completed and debugged as described above. It has accurately demonstrated all of the null results that we were expecting. Unfortunately, user error prevented it from what could have been its most insightful result this summer. As we played with the use of a prism to alter the optical pathlength, the simulation was

giving a positive result. After several weeks of experimentation, some trigonometry proved that all setups should give null results. The simulation was not wrong, however, but the prism had been placed so the beam was exactly hitting it on its tip. Such a singularity between refracting planes was ruining the calculation precision, allowing the simulation to return a false positive. Once the prism was moved to the correct location, the simulation returned the now-expected null result. Several weeks of working time, though, were lost due to this mistake that could and should have been avoided by this simulation's results.

4 Straightness Monitor Design

The straightness monitor itself was designed on the concept of measuring distance with a laser interferometer. A laser interferometer splits coherent laser light into two beams; when they are later recombined, they are no longer in phase because they have traveled different distances. The precision of a normal laser interferometer is on the order of a quarter wavelength—about 150nm for red laser light—since distances are interpreted by fringes of constructive and destructive interference. Our straightness monitor, however, uses a so-called heterodyne laser. Heterodyne lasers emit two very close frequencies of light, one polarized horizontally and the other polarized vertically. When the light is recombined at the pickup, one polarization state will be out of phase with the other; by measuring the difference in phase between polarizations, the data acquisition software can obtain distance measurements with a precision of about 10nm .

We worked on monitoring two varieties of motion: Position of interferometer with respect to the beamline and position of beam with respect to the interferometer. With the assumption that both the accelerator beam and the laser beam are stationary, all distances in the

system can be found. Progress on each component of the straightness monitor, as well as plans for future work, are detailed in the sections to follow.

4.1 Transverse Beamline Motion

First, we want to be able to record the position of the beamline with respect to the interferometer. This is likely the more important measurement, in that it should eliminate the beamline vibrations of several microns. When we began work on this project, several test runs had already been run at the Stanford Linear Accelerator (SLAC) with an early model of this straightness monitor. In the early monitor, special birefringent beamsplitters were in use; these naturally split the beam into the two polarizations, but it required that the beam be separately divided for each BPM.

We wanted a system that would allow for all of the beamsplitters to be collinear, such that the same laser beam provided the reference for all BPMs. This required a change in setup so that both the measurement and reference arms of each interferometer were orthogonal to the main laser beam (see figure, Appendix A). The beamsplitter corresponding to each BPM must transmit a larger portion of the light than it will reflect, allowing a beam with sufficient intensity to span the entire beamline. At the time of this writing, we had experimented with both 50-50 and 92-8 beamsplitters; the former do not transmit enough light, while the latter do not reflect enough. Data from these experiments suggest that the optimal beamsplitter should reflect 20-30% of incident light. Additionally, both polarization states must be transmitted, so ordinary beamsplitters must replace their birefringent counterparts. As seen in the figure, polarizing filters are placed on the actual interferometer arms to separate the polarization states.

4.2 Transverse Laser Motion

If we assumed that the beamsplitters were stationary, the above straightness monitor would suffice. However, we also wanted to incorporate some method for measuring the position of the beamsplitter with respect to the laser beam, and such a test had not been performed during previous runs at SLAC. Due to the forty-five degree angle of the beamsplitters, the interferometer was normally blind to transverse laser motion. We thought that the insertion of a glass prism would break the translation symmetry, thus allowing us to measure the stability of the beamsplitters.

We tried several configurations for the glass prisms (see figures, Appendix A), but all yielded a null result. Even with the prism, the translation symmetry held. As mentioned above, my simulation—and all of our intuition—led us to believe that we should see the symmetry broken, so we continued testing new configurations. In the end, the problem rested in the difference between the Cartesian pathlength and the optical pathlength. While the Cartesian pathlength varies, the optical pathlength remains unchanged under transverse laser motion. This can even be reasoned intuitively: A laser beam—which has a finite width, analogous to a transverse shift—remains entirely coherent as it passes through a refractive surface. Afterward, we found the flaw in the simulation that led to the false positive, verifying that we should still expect a null result even with glass prisms.

4.3 Future Work

For the transverse beamline motion monitor, on the one hand, we will focus on the continuation of this summer's success. The first goal should be the determination of optimal beamsplitter; enough laser light must be transmitted for the laser beam to span the entire beamline, but enough must be reflected for each interferometer to work individually. Following

this, a prototype needs to be constructed and tested. Future experimental runs will no longer be in SLAC, due to a shutdown of End Station A at the facility. Currently, the Japanese laboratory KEK is the leading candidate for a replacement test facility, but plans may not reach fruition for a couple years.

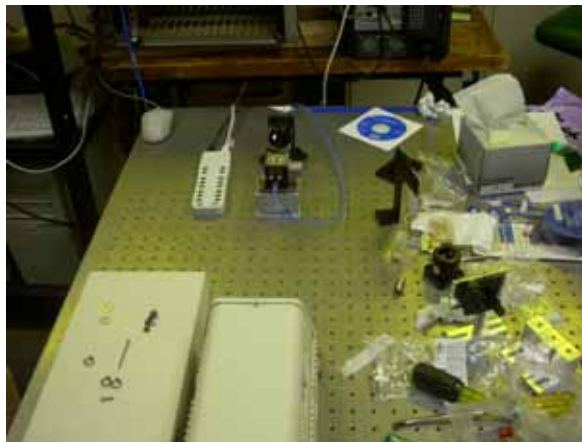
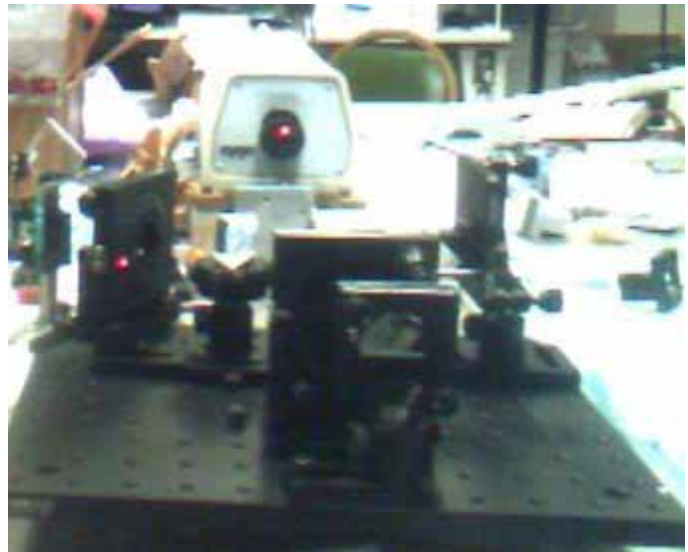
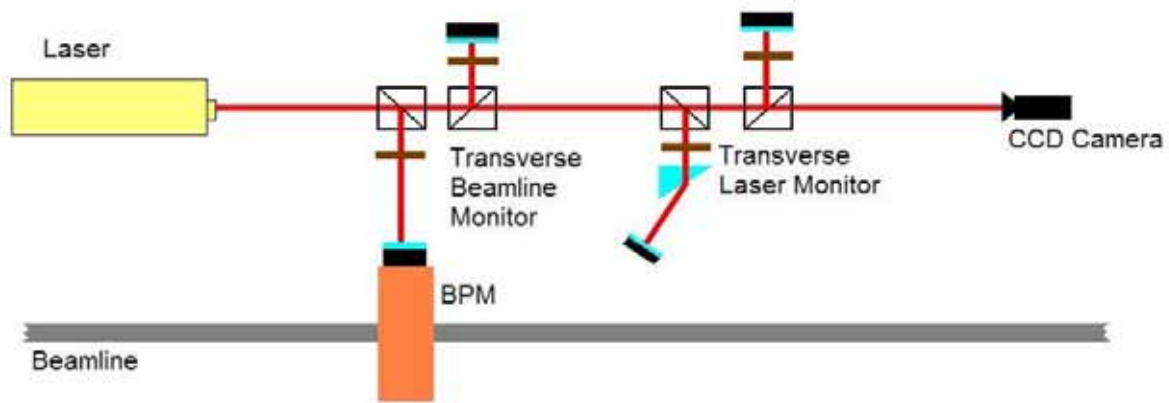
For the transverse laser motion monitor, on the other hand, we need an entirely new measurement method. We investigated one possibility, a CCD camera at the end of the beamline, during our work this summer. In this technique, a CCD camera would be placed in the beamline following the last beamsplitter. It would record the beam and track its center of intensity, which would measure the transverse motion of the laser. We also considered a possibility for measuring angular tilting motion of the laser based on a concept used in the Laser Interferometry Space Antenna (LISA) experiment. With a heterodyne laser beam, a beamsplitter, and two CCD cameras, one can measure the phase shift between beams with the cameras. The magnitude of the phase shift can be used to determine the angular offset of the measurement beam with respect to the reference beam.

5 Conclusions

Work on both laser interferometry monitors progressed this summer, with varying levels of success. First and foremost, a simulation was developed that works well in most situations, accurately predicting the pathlength variations. Development of failsafe mechanisms for this simulation would be useful, helping to prevent another fatal user-induced error like the improperly placed prism. Additionally, we showed that the development of a series of transverse beamline motion monitor with a single laser beam is feasible. Work will be required to find beamsplitters with the proper transmission-reflection ratio, but development of a working multi-

interferometer setup should be relatively straightforward given the work from this summer. Finally, we demonstrated that a glass wedge—or any series of optical components—cannot be used as a transverse laser motion monitor. Work continues on other methods for measuring this laser motion, such as a CCD camera at the end of the beam.

6 Figures and Pictures



Left to Right, From Top to Bottom:
 Straightness Monitor Schematic
 Original Transverse Laser Motion Monitor
 Final Transverse Beamline Motion Monitor
 Final Transverse Laser Motion Monitor